Current Research in Food Science 10 (2025) 100984

Contents lists available at ScienceDirect

Current Research in Food Science

journal homepage: www.sciencedirect.com/journal/current-research-in-food-science

Enhancing water solubility of phytosterols through Co-amorphization with food-grade coformers

Yuxin Li [a], Yingting Luo [a], Xuening Song [a], Yuzhuo Wang [a], Simiao Liu [a], Fazheng Ren [a,b,c], Lingyan Kong [d], Hao Zhang [a,b,c,*]

[a] College of Food Science and Nutritional Engineering, China Agricultural University, Beijing, 100083, China
[b] Beijing Laboratory of Food Quality and Safety, Department of Nutrition and Health, China Agricultural University, Beijing, 100091, China
[c] Food Laboratory of Zhongyuan, Luohe, 462300, Henan, China
[d] Department of Human Nutrition, Hospitality and Sport Management, The University of Alabama, Tuscaloosa, 35487, Alabama, USA

ARTICLE INFO

Handling Editor: Professor Aiqian Ye

Keywords:
Phytosterol
Co-amorphous
Solubility
Nicotinamide
Lyophilization

ABSTRACT

Phytosterols (PS) offer significant health benefits in human diet, but its poor solubility limits its effectiveness and application. This study explored enhancing PS solubility by testing thirteen food-grade coformers, three preparation methods and proportions screening to obtain the optimal formulation. Nicotinamide (Nic) was identified as the most effective coformer. A 20:1 (w/w) PS-Nic co-amorphous (CM) mixture, prepared via freeze-drying, achieved a solubility of 1536.4 μg/mL, significantly higher than pure PS. X-ray diffraction and differential scanning calorimetry confirmed the amorphous state of the mixture. Fourier-transform infrared, Raman, and ^{1}H NMR spectroscopies, along with molecular dynamics simulations, revealed strong intermolecular interactions between PS and Nic. The PS-Nic CM demonstrated up to 60% *in vitro* dissolution and release within 2 h and maintained stable after storage at 4 °C for 6 months and under accelerated conditions equivalent to 10 months at room temperature. In sum, the crystal structure of PS was altered, and formed a co-amorphous system by using Nic as the optimal ligand via lyophilization to increase solubility. These findings suggest that the PS-Nic CM system has potential applications in functional foods, offering a feasible strategy to enhance the bioavailability of PS.

1. Introduction

Phytosterols (PS), a class of sterol compounds in plant cells, belongs to the triterpene family. The number of methyl groups at C_4 and the type of C_{17} side chain determine the specific type of PS (Moreau et al., 2018). The most common types of PS are β-sitosterol, campesterol, and stigmasterol, with the former two accounting for more than 50% in typical human diets (Yang et al., 2019). These naturally occurring compounds have gained significant attention due to their potential health benefits, particularly in lowering cholesterol levels and improving heart health. PS can competitively inhibit the formation of dietary mixed micelles of cholesterol, affecting its intestinal absorption and transport capacity and leading to the excretion of cholesterol via faeces (Matsuoka, 2022). This effect is attributed to the structural similarity between PS and cholesterol. The minimum daily intake dose of PS for lowering blood cholesterol has been reported to be 800 mg (Matsuoka et al., 2004). In addition to their cholesterol-lowing properties, PS demonstrate anti-inflammatory activity. Epidemiological studies have revealed that PS intake is negatively associated with the occurrence of certain cancers, such as ovarian and gastric cancer (De Stefani et al., 2000; Mccann et al., 2003). Although PS are widely found in vegetable oils, cereals, nuts, vegetables, and fruits, the daily dietary intake of PS in different countries ranges from 150 to 450 mg, which is insufficient to meet the minimum effective cholesterol-lowering dosage of 800 mg/day. Therefore, PS supplements or PS-fortified foods are often required to achieve the desired health benefits.

However, PS typically have relatively large molecular weights, around 400–500 g/mol and high melting points, ranging from 120 °C to 150 °C, and is thus poorly soluble in both water and oil. The poor water solubility of PS is due to their polycyclic steroid nuclei and hydrophobic side chains at C17, while their oil solubility is limited by the presence of the C3-hydroxyl group. To enhance their solubility and bioavailability,

* Corresponding author. College of Food Science and Nutritional Engineering, China Agricultural University, Beijing, 100083, China.
E-mail addresses: s20203060977@cau.edu.cn (Y. Li), s20213061018@cau.edu.cn (Y. Luo), 2020306100616@cau.edu.cn (X. Song), wyz@cau.edu.cn (Y. Wang), s20233061224@cau.edu.cn (S. Liu), renfazheng@cau.edu.cn (F. Ren), lingyan.kong@ua.edu (L. Kong), zhanghaocau@cau.edu.cn (H. Zhang).

https://doi.org/10.1016/j.crfs.2025.100984
Received 8 December 2024; Received in revised form 17 January 2025; Accepted 20 January 2025
Available online 21 January 2025

various methods, e.g., esterification and emulsification, have been employed. Esterification and other chemical modification methods involve complex processes and the use of toxic and non-food-grade reagents, which limit the application of modified PSs in the food industry. Moreover, esterified PS must be hydrolyzed in the intestine to release free PS that acts on lowering cholesterol. Additionally, researchers have developed water-soluble PS using emulsifiers such as the Tween series, isolated protein, and phosphatidylcholine (Acevedo-Estupiñan et al., 2019; Yamamura et al., 2000). Yet, PS can be unstable in emulsions due to its larger particle size when crystallized. Furthermore, certain nanotechnology enabled methods can reduced the particle size of PS nano-complex, but they usually exhibits low loading capacity (Feng et al., 2021).

A co-amorphous (CM) system is created by disrupting the three-dimensional, long-range ordered structure of crystalline substances. In the CM system, lattice energy does not need to be overcome during dissolution, which can improve the solubility of various substances (Hancock and Zografi, 1997). In recent years, CM technology has been widely applied to solubilisation of natural bioactive compounds, functional food ingredients and drugs (Garbiec et al., 2023; Oyama et al., 2024; Song et al., 2024). In this study, we aim to investigate various methods, i.e., rotary evaporation, spray drying, and freeze-drying, for preparing CM systems with different mass ratios of PS and food-grade coformers, with the goal of increasing the water solubility of PS. These co-formers were chosen because they are well soluble in water, safe, legal and commonly used as additives in food production. To identify the optimal conditions, we used X-ray diffraction and differential scanning calorimetry were used to study the crystal structure and thermodynamic changes of the samples, respectively. Scanning electron microscopy was employed to observe the surface morphology and particle size of the samples. The interactions between the compounds in the samples were investigated by Fourier-transform infrared absorption, Raman, and nuclear magnetic resonance spectroscopies. Additionally, molecular dynamics simulations were used to determine the interaction sites between the compounds. Finally, the dissolution and stability of the samples were evaluated *in vitro*.

2. Materials and methods

2.1. Materials

PS (95%, food grade) was purchased from Xi'an ML Biological Technology Co., Ltd. (Shanxi, China). Coformers, including arginine, nicotinamide, methionine, isoleucine, sorbitol, stevioside, lactitol, fructose, lactose, xylose, citric acid, malic acid and ascorbic acid (≥98%, food grade) were purchased from Shandong Pingju Biotechnology Co., Ltd. (Shandong, China). Absolute ethanol was purchased from Tianjin Zhiyuan Chemical Reagent Co., Ltd. (Tianjin, China). Chromatography pure acetonitrile and methanol were purchased from Beijing Mairuida Technology Co., Ltd. (Beijing, China). KBr (spectrum pure) was purchased from Shanghai Macklin Biochemical Technology Co., Ltd. (Shanghai, China). Other reagents used were of analytical grade and purchased from Tianjin Yongda Chemical Reagent Co., Ltd. (Tianjin, China).

2.2. Preparation of highly water-soluble PS mixtures

Arginine (Arg), methionine (Met), isoleucine (IsoLeu), sorbitol (Sob), stevioside (Ste), lactitol (Lacl), fructose (Fru), lactose (Lac), xylose (Xyl), citric acid (CA), malic acid (MA), ascorbic acid (AA), and nicotinamide (Nic), which are common small-molecule raw materials used in the food industry, were used as coformers for screening PS solubilizing via rotary evaporation. PS was dispersed in absolute ethanol, and the above mentioned coformers were dissolved in deionized water, respectively. After the PS and the corresponding coformer of equal mass ratio became miscible, the solution was heated to 75 °C until it was clarified. The resulting solution was evaporated at 75 °C and dried in a vacuum drying oven at 60 °C.

The optimal coformer was selected based on the results, and it was used to study the effects of spray drying and freeze-drying preparation methods and the effects of the PS-coformer proportion on the solubility of PS. The spray drying preparation was performed using a RE 2000A spray dryer purchased from Shanghai Yarong Biochemistry Instrumentfactory (Shanghai, China) under the following conditions: inlet temperature = 160 °C ± 5 °C; outlet temperature = 90 °C ± 5 °C; feed rate = 22%; and atomising gas flow rate = 42 mm (Alvarez-Henao et al., 2023). A Delta 2–24 LSCplus freeze dryer manufactured by Marin Christ (Osterode, Lower Saxony, Germany) was used, and the lyophilization conditions were as follows: temperature = −80 °C ± 10 °C; time = 96–168 h. The recommended daily dosages of PS and optimal conformer Nic are determined to be 2 g and 16–100 mg, respectively. Hence, 20:1 and 100:1 (w/w) PS-Nic physical mixtures were prepared by grinding them into a powder, and their performances were compared. All samples were stored at 4 °C until further testing. Moreover, it was observed during the experiment that individual PS cannot be transformed into the amorphous state by the same preparation methods. Hence, we only measured pure PS as the crystalline references.

2.3. Solubility studies using high-performance liquid chromatography (HPLC)

Quantitation of PS. A standard solution (0–200 μg/mL) of PS was prepared by dissolving it in 5:1 (v/v) ethanol/water. The PS content in this solution was determined via HPLC (Careri et al., 2001) using a Waters XBridge^{TM} C_8 column (4.6 × 250 mm, 5 μm) at 35 °C with a mobile phase of 86% acetonitrile and 14% water. The flow rate of the mobile phase was 1 mL/min, the sample volume was 20 μL, and the sample peak area at 208 nm was measured. The peaks of the three main components of the PS mixture (β-sitosterol, stigmasterol, and campesterol) were observed in the chromatogram. These were compared with those in the calibration curve plotted using PS solutions of 0–200 μg/mL concentrations. A supersaturated solution was obtained by mixing the powder with the same volume of water. The solution was shaken at 200 rpm in a water bath at 25 °C for 24 h (Meng et al., 2012). The solubility of PS in this supersaturated solution was determined via the above-mentioned HPLC method. The mixture with the optimal solubility was selected for subsequent characterisation.

2.4. Characterisation of the highly water-soluble PS mixture

2.4.1. X-ray diffraction (XRD)

XRD patterns were acquired using an XD-3 X-ray diffractometer (Persee Chemicals, China) with Cu radiation at room temperature at a tube voltage and an amperage of 36 kV and 20 mA, respectively, over a 2θ range of 5°–30°. The scanning speed was 4°/min, and the step size was 0.02° (Gan et al., 2022).

2.4.2. Differential scanning calorimetry (DSC)

A DSC-60 differential scanning calorimeter (Shimadzu, Japan) was used. Samples (3–5 mg) were heated in an aluminium crucible at a heating rate of 10 °C/min from 25 °C to 200 °C with an N_2 flow rate of 50 mL/min (Liu et al., 2023). The result was expressed as heat flow per unit weight of the sample (mW/mg).

2.4.3. Scanning electron microscopy (SEM)

The surface morphology of the samples was observed using a SU3500 SEM microscope (Hitachi, Japan). Prior to acquiring the SEM images, each sample was fixed to the sample table with conductive tape and sputter-coated with Au.

2.4.4. Fourier-transform infrared spectroscopy (FTIR)

FTIR spectroscopy were obtained using a Frontier™ Fourier Infrared

Spectrometer (PerkinElmer, USA). Each sample was scanned at a resolution of 4 cm^{-1} for 64 scans over a frequency range of 400–4000 cm^{-1}.

2.4.5. Raman spectroscopy

A LabRAM HR Evolution micro confocal laser Raman spectrometer (Horiba, France) was used to acquire the spectra over a range of 400–3500 cm^{-1} with 100% intensity and an excitation wavelength of 633 nm (Biniek et al., 2018).

2.4.6. Molecular dynamics (MD) simulations

The PS and Nic structures were downloaded from PubChem (https://pubchem.ncbi.nlm.nih.gov/). Materials Studio 2019 software (Accelrys, USA) was used for geometric optimisation of the structures, with the maximum number of iterations set to 10,000 at an amorphous cell code. A 20:1 (w/w) PS-Nic co-amorphous system was constructed in cubic cells with periodic boundary conditions and fine quality parameters. The reaction was simulated using the isotherm-isobaric (NPT) and the canonical ensemble (NVT) with a step width of 1.0 fs. The radial distribution function (RDF) was calculated and analysed after the reaction parameters were balanced (Li et al., 2022).

2.5. In vitro release of PS

Ten mg each of PS and highly water-soluble PS, as well as an equivalent amount of the physical mixture (PM) of the 20:1 (w/w) PS-Nic mixture, were separately dissolved in 100 mL of 0.1% Tween 80 aqueous solution and continuously stirred with a magnetic stirrer at 37 °C and 100 rpm (Yang et al., 2018). 1 mL of the stirring solution was collected at 0, 5, 15, 30, 60, 90, 120, 180, 300 min. Then, an equal amount of 0.1% Tween 80 aqueous solution was added. The solubility of PS in the collected samples was determined by the same HPLC procedure described in Section 2.3. Triplicate measurements were acquired at each time point and expressed as the ratio (%) of released PS to input PS.

2.6. Storage stability

The highly water-soluble PS mixture was placed at 4 °C, 0% relative humidity (RH; containing anhydrous $CuSO_4$) at room temperature, and 75% RH (containing saturated NaCl solution) at 40 °C, respectively (Wegiel et al., 2014), to simulate the potential environments of product storage in the real world. The powder was collected at different time points for XRD analysis to observe the change in crystallinity.

2.7. Statistical analysis

All measurements were performed in triplicate, and the mean ± standard deviation (SD) values were calculated. A *t*-test was performed among groups, and one-way analysis of variance (ANOVA) with Duncan's multiple range test was performed within groups using SPSS 22 software (SPSS Inc., Chicago, IL, USA). The differences were considered significant at $p < 0.05$.

3. Results and discussion

3.1. Preparation of a highly water-soluble PS mixture

PS was almost insoluble and only 0.022 ± 0.003 mg/mL of PS dissolved in distilled water at 25 °C for 24 h was detected via a high-sensitivity gas chromatograph (Meng et al., 2012). However, the addition of different coformers increased the water solubility of PS to different extents (Fig. 1). Among the tested amino acids, Arg had the highest solubilizing effect (457.3 μg/mL) on PS, followed by IsoLeu and Met. Generally, basic amino acids such as Arg are better co-amorphous coformers for acidic compounds, while non-polar amino acids such as Met have a negligible effect on solubility (Kasten et al., 2019). Among the tested sugars and sugar alcohols, Xyl had the highest solubilizing effect on PS (485.8 μg/mL), while others had a negligible effect on PS solubility. This could be explained by the larger particle sizes of sugars and sugar alcohols upon aggregation, which was not conducive to dissolution (Kamiya et al., 2010). Among the tested acids, MA had the highest solubilizing effect on PS (326.8 μg/mL), followed by CA and AA. Notably, Nic demonstrated the highest solubilizing effect on PS (633.4 μg/mL; $p < 0.05$). This is consistent with previous reports, where Nic significantly improved the solubility of the insoluble compounds valsartan (Turek et al., 2021) and carbamazepine (Liu et al., 2012). This had been attributed to the ability of Nic to destroy the structure of water in solution and/or to form complexes or hydrogen bonds with certain compounds based on electron donor-acceptor interactions (Ahuja et al., 2007). Hence, a PS-Nic mixture was used for further experiments.

Rotary evaporation (RE), freeze drying (FD), and spray drying (SD) are widely used in research laboratories and industrial manufacturing to prepare mixtures. In this study, we compared the effect of the preparation method for PS-Nic mixtures of different mass ratios on the solubility of PS. As the concentration of PS increased in the PS-Nic mixture, RE decreased the solubility of PS whereas FD and SD first increased and then decreased the solubility of PS (Fig. 2). The FD-PS with a 20:1 (w/w) ratio exhibited the highest solubility (1536.4 μg/mL; $p < 0.05$). This might be attributed to the highly porous PS surface of PS-Nic obtained via FD (Asare-Addo et al., 2019). Generally, as the proportion of polymers increased in mixtures of polymers and insoluble compounds, the solubility of the insoluble compounds increased, due to the coating effect of hydrophilic polymers and their strong surface activity (Muthu et al., 2019). However, a high proportion of polymers negatively affected drug modification ability and drug-polymer interactions (Pham et al., 2019). A higher proportion of small-molecule coformers in the mixture did not improve the solubility of curcumin and ascorbic acid (Bhagwat et al., 2021), which may be attributed to coformer-insoluble compound interactions and the granular properties of the products. In summary, the 20:1 (w/w) PS-Nic powder prepared via FD demonstrated the highest PS solubility and, hence, was selected for subsequent analyses.

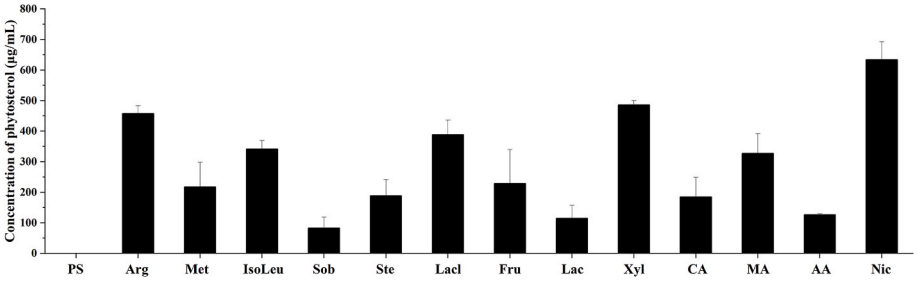

Fig. 1. Screening different coformers to determine highly water-soluble phytosterol (PS) using rotary evaporation. The data shown are the average of triplicate measurements.

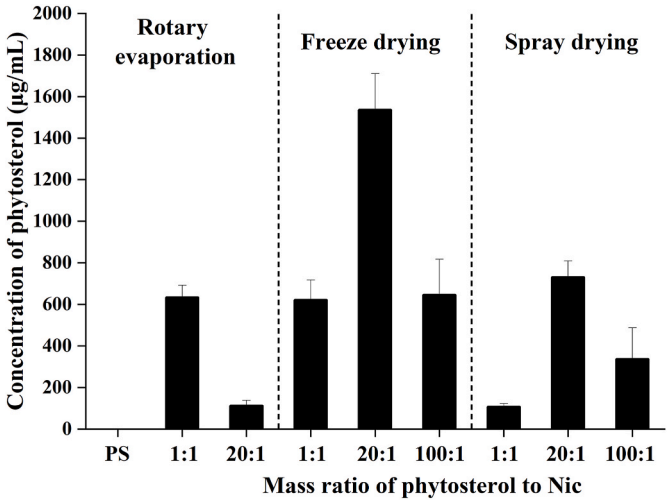

Fig. 2. Screening the solubility of PS-Nicotinamide (Nic) mixtures prepared using different mass ratios and different methods. The data shown are the average of triplicate measurements.

3.2. Characterization of the highly water-soluble PS mixture

3.2.1. X-ray diffraction (XRD)

XRD can effectively detect changes in the crystal structure and crystallinity of the samples. The XRD patterns of PM, lyophilizate (CM) and their raw materials PS and Nic are shown in Fig. 3(A). The diffraction peaks of the raw PS were observed at $2\theta = 5°$, 15.1°, 16.0°, and 16.9°, in agreement with a previous report (Rozner et al., 2009). The Nic showed diffraction peaks at $2\theta = 14.8°$, 22.3°, 23.4°, 25.4°, 25.9°, and 27.4°, which is also consistent with a previous report (Ding et al., 2023). The PM pattern contained both PS and Nic patterns superimposed on one another, and no new peaks were observed, showing that PS and Nic did not form any new crystals. The CM pattern, otherwise, exhibited no diffraction peaks, indicating that its spatial structure was altered and successfully transformed into the co-amorphous forms.

3.2.2. Differential scanning colorimetry (DSC)

DSC is typically used to analyze the thermal behavior of materials. In this study, DSC was used to observe the thermodynamic changes in the PS-Nic CM. The melting points of PS and Nic were approximately 135 °C and 132 °C, respectively (Fig. 3(B)), which were consistent with previous reports (Ribeiro et al., 2016; Tawfeek et al., 2020). However, the melting point of PM was 130 °C which could be attributed to an overlap of the melting point peaks of PS and Nic. Moreover, the increasing temperature might have melted the components of PM, leading to in-situ aggregation (Telange et al., 2017). However, CM does not exhibit any melting endotherm in its DSC thermogram, indicating good miscibility of PS and Nic (Borde et al., 2021). Similarly, the melting endotherm of curcumin disappeared in the DSC curve of the co-amorphous curcumin powder (He et al., 2019). These results suggested that PS was uniformly dispersed with the coformer in the amorphous state.

3.2.3. Scanning electron microscopy (SEM)

SEM is used to observe the surface morphology of materials. The SEM images of the PS, Nic, PM, and CM revealed their overall morphology (Fig. 4(A)–(D)). PS existed as nearly spherical crystal blocks (under 20 μm) with irregular edges, while Nic showed elliptic crystal blocks (50–100 μm) with smooth edges but many surface layers (Fig. 4(E)–(H)). PM exhibited the morphology of both PS and Nic with varied particle sizes, whereas CM demonstrated a completely different morphology. The surface of CM was smooth and elastic, leading to lower particle sizes and increased surface area of PS. This is a well-known characteristic of a mixture of a poorly water-soluble compound and a hydrophilic coformer in a co-amorphous system. Hence, the introduction of the coformer after lyphilization helped in the solubilisation of the insoluble compound (Zhang et al., 2018).

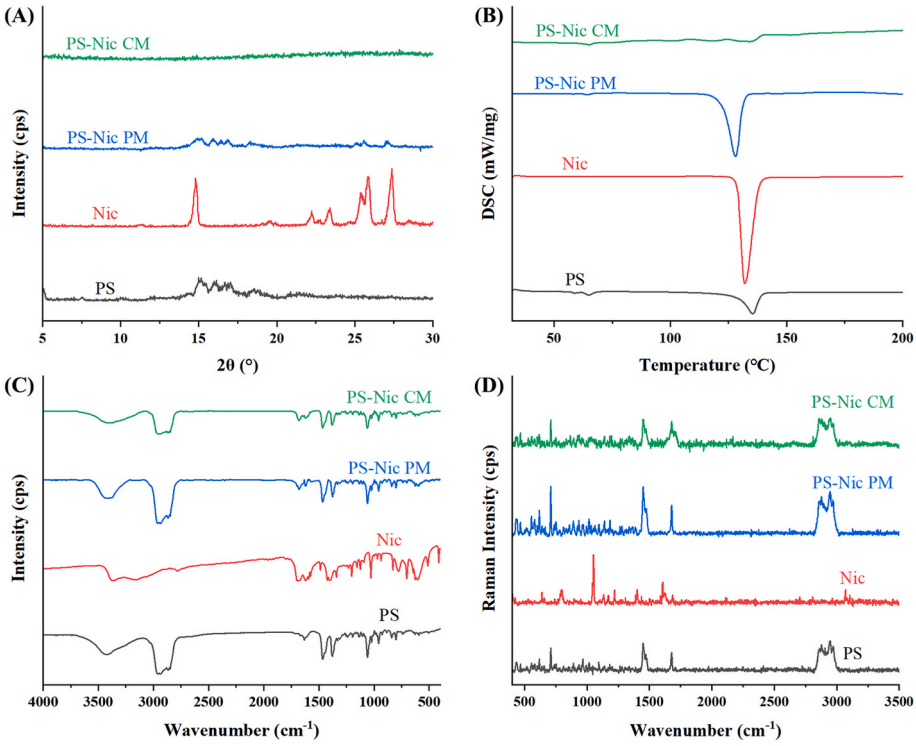

Fig. 3. (A) XRD, (B) DSC, (C) FTIR and (D) Raman spectra of PS, Nic, their 20:1 (w/w) physical mixture (PM), and their 20:1 (w/w) freeze-dried co-amorphous product (CM).

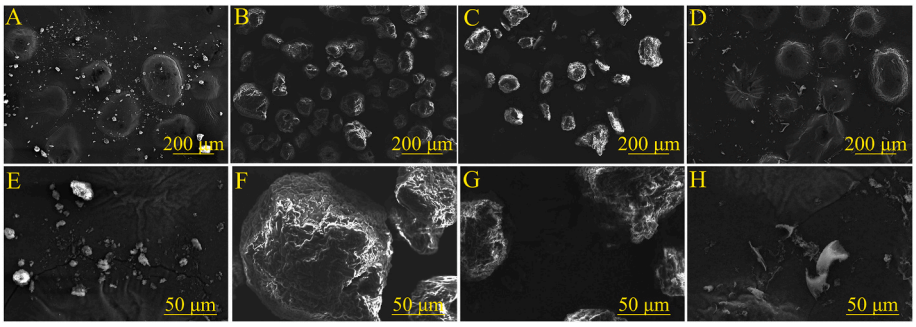

Fig. 4. Scanning electron microscopy images of (A, E) PS, (B, F) Nic, (C, G) 20:1 (w/w) PS-Nic PM, and (D, H) 20:1 (w/w) freeze-dried PS-Nic CM at 200 × and 50 × magnification, respectively.

3.2.4. Fourier transform infrared spectroscopy (FTIR)

FTIR is used to characterise the interactions between substances. As shown in Fig. 3(C), the major IR bands of PS were 3423 cm^{-1} (O–H stretching vibration), 2850–2935 cm^{-1} (C–H_3 and C–H_2 stretching vibration), 1464 cm^{-1} (C–H_2 bending vibration), 1376 cm^{-1} (C–H_3 bending vibration), and 1057 cm^{-1} (polycyclic ring vibration) (He et al., 2012). The characteristic IR bands of Nic were 3367–3164 cm^{-1} (N–H tensile vibration), 3060 cm^{-1} (C–H tensile vibration), 1680–1698 cm^{-1} (C=O vibration), 1619 cm^{-1} (N–H_2 vibration), 1423–1593 cm^{-1} (pyridine ring tensile vibration), 1390 cm^{-1} (C–N vibration), 1202 cm^{-1} (C–C vibration), 1029 cm^{-1} (ring deformation vibration), and 778–828 cm^{-1} (C–H vibration) (Lin et al., 2014). The PM spectra contained peaks of both PS and Nic, which indicated the absence of any new bond formed between PS and Nic. In contrast, the O–H and N–H vibration bands of CM were significantly broadened and weakened compared to those of PM. In addition, the O–H band of PS shifts to 3371 cm^{-1}, and the C–H_3 and C–H_2 stretching vibration bands of PS (2850–2935 cm^{-1}) were significantly weakened in the CM spectrum. The C=O and C–N vibration peak intensities, corresponding to Nic, were also slightly lower in the CM spectrum. Overall, the FTIR spectral features of co-amorphous systems were peak displacement and peak broadening (Heinz et al., 2009), which could be attributed to the crucial role played by the interactions of O–H, N–H, C=O, C–N, and other functional groups in the transformation of the crystalline state to an amorphous state.

3.2.5. Raman spectroscopy

Raman spectroscopy and FTIR complement each other and reveal the structural properties and interactions between samples. As shown in Fig. 3(D), the characteristic Raman peaks of PS were 708–962 cm^{-1} (OH stretching), 1452 cm^{-1} (C–H_2 deformation), 1678 cm^{-1} (C=C stretching), and 2873–2968 cm^{-1} (C–H vibration). The characteristic Raman peaks of Nic were 800 cm^{-1} (N ring in the pyridine nucleus), 1053 cm^{-1} (C=O–NH_2), and 1603 cm^{-1} (C=N and C=C) (Pal et al., 1998). The PM Raman spectrum was apparently the overlap of the Raman spectra of PS and Nic. However, the peak intensities of Nic were weak owing to its low proportion in the mixture. In contrast, the CM spectral peaks were significantly weakened or even disappeared. Moreover, the C=O–NH_2 and C=C elongation peaks at 1053 cm^{-1} and 1683 cm^{-1}, respectively, significantly widened. Similar peak shifts and peak weakening have been observed for amorphous curcumin (Meng et al., 2015), indicating interactions between the components of the mixture that transformed the crystal into an amorphous state.

3.2.6. Molecular dynamics (MD) simulations

MD simulations reveal potential interaction sites between reactants and, thus, complement experimental data. The main components of PS (β-sitosterol, stigmasterol, and campesterol) were considered analysis objects in the MD simulations. According to PubChem data, β-sitosterol, stigmasterol, and campesterol contain one hydrogen bond donor and one hydrogen bond acceptor, whereas Nic contains one hydrogen bond donor and two hydrogen bond acceptors. These sites were used as analysis objects to determine the possible interactions between β-sitosterol, stigmasterol, campesterol, and Nic using the radial distribution function (RDF). The main intermolecular interactions within 3.5 Å were hydrogen bonding or van der Waals forces (Li et al., 2022). Five intermolecular interactions were observed between the PS and Nic (Fig. 5): (1) C=O of Nic and O-H of β-sitosterol; (2) N_1 of Nic and O-H of β-sitosterol; (3) N_1 of Nic and O-H of stigmasterol; (4) C=O of Nic and O-H of campesterol; and (5) N_1 of Nic and O-H of campesterol. The minimum distance and the maximum probability force of 1.78 Å were present between N_1 of Nic and O-H of stigmasterol, which is the typical hydrogen bonding distance. Moreover, the two interactions between Nic and β-sitosterol were within 3.5 Å, which lies within the probable interaction distance. The smaller the distance and the greater the g(r) value, the stronger the interaction. The interactions between the C=O and O-H groups within an apigenin-oxymatrine co-amorphous mixture appeared as an interaction peak at 1.87 Å (Li et al., 2022). Furthermore, different compounds and reaction states could have different interactions even at the same site. The functional groups that participate in the five intermolecular interactions identified via our MD simulations were consistent with the functional groups identified in our spectral analysis. Therefore, these PS-Nic interactions may have induced the formation of a co-amorphous system, thus promoting the solubility of PS.

3.3. In vitro release

The *in vitro* release of PS, PS-Nic PM, and PS-Nic CM was simulated under conditions of high concentration differences between the substances on both sides of the gastrointestinal membrane. The 0.1% Tween 80 aqueous solution was used as the release medium to create a leak tank condition for PS because of its extremely low water solubility (Yang et al., 2018). However, PS and the PS in PM did not dissolve even after 5 h, while the PS in CM was gradually released to nearly 60% within 2 h (Fig. 6). This dissolution was significantly higher than that of PS and PS in PM ($p < 0.05$) but did not significantly increase between 2 and 5 h ($p > 0.05$). In addition, PS and the PS in PM were suspended in solution even after continuous agitation in a 37 °C water bath, whereas the PS in CM slowly seeped from the top and slowly dispersed in the whole solution, turning the solution into a light white color. Co-amorphization significantly reduced the particle size of the PS, facilitating strong intermolecular interactions, which destroyed the ordered crystal structure. All these factors enabled the rapid dissolution and, consequently, the high *in vitro* release of PS.

3.4. Storage stability

A co-amorphous system is typically prone to recrystallization, thus destabilizing it. Therefore, the XRD analysis performed immediately after preparation (0 day) confirmed the amorphous form of PS-Nic CM.

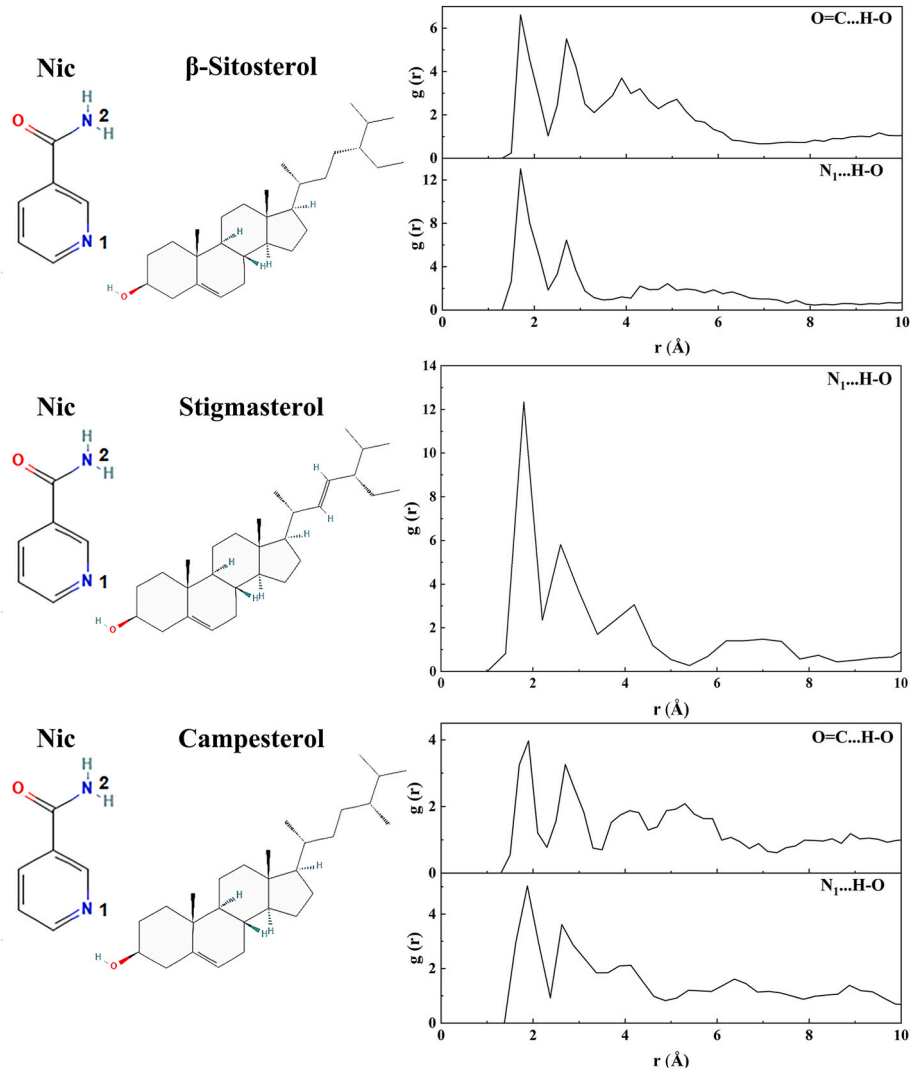

Fig. 5. Molecular dynamics simulations of 20:1 (w/w) freeze-dried PS-Nic CM.

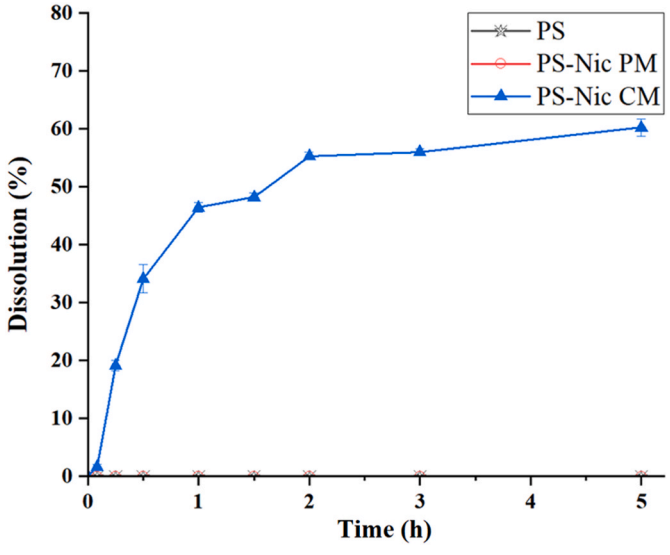

Fig. 6. In-vitro release of PS, 20:1 (w/w) PS-Nic PM, and 20:1 (w/w) freeze-dried PS-Nic CM.

Obviously, the high intensity crystalline peaks were absent from their XRD patterns, in comparison with the PS, Nic and PS-Nic PM (Fig. 7). And we evaluated the stability of the PS-Nic system under different storage conditions using XRD. The PS-Nic CM did not recrystallize and maintained its amorphous state even after being stored at 4 °C for 6 months and at room temperature for 2 months (Fig. 7(A)–(B)), which suggested good stability. When PS-Nic CM was subjected to accelerated storage conditions for 2.5 months (equivalent to the storage condition of 10 months at room temperature, 25 °C, and 60% RH), its XRD patterns did not exhibit any diffraction peaks (Fig. 7(C)), indicating the absence of crystal structure change. A similar phenomenon has been reported for the baicalin-histidine co-amorphous system stored at room temperature for 6 months (Jangid et al., 2020), which could be attributed to the strong interaction between the components.

Stable amorphous systems typically require the addition of a high proportion of polymers or crystallization inhibitors, which reduces the proportion of the main component and limits miscibility between the main component and the polymers. In addition, the high hygroscopicity of polymers makes the processing of the mixture difficult. Nevertheless, if low-molecular-weight coformers are used in the co-amorphous system, the issue of substance-polymer miscibility can be resolved. Moreover, low-molecular-weight coformers might produce stronger intermolecular interactions, such as hydrogen bonds and ionic interactions, thus reducing molecular mobility (Lim et al., 2022) and

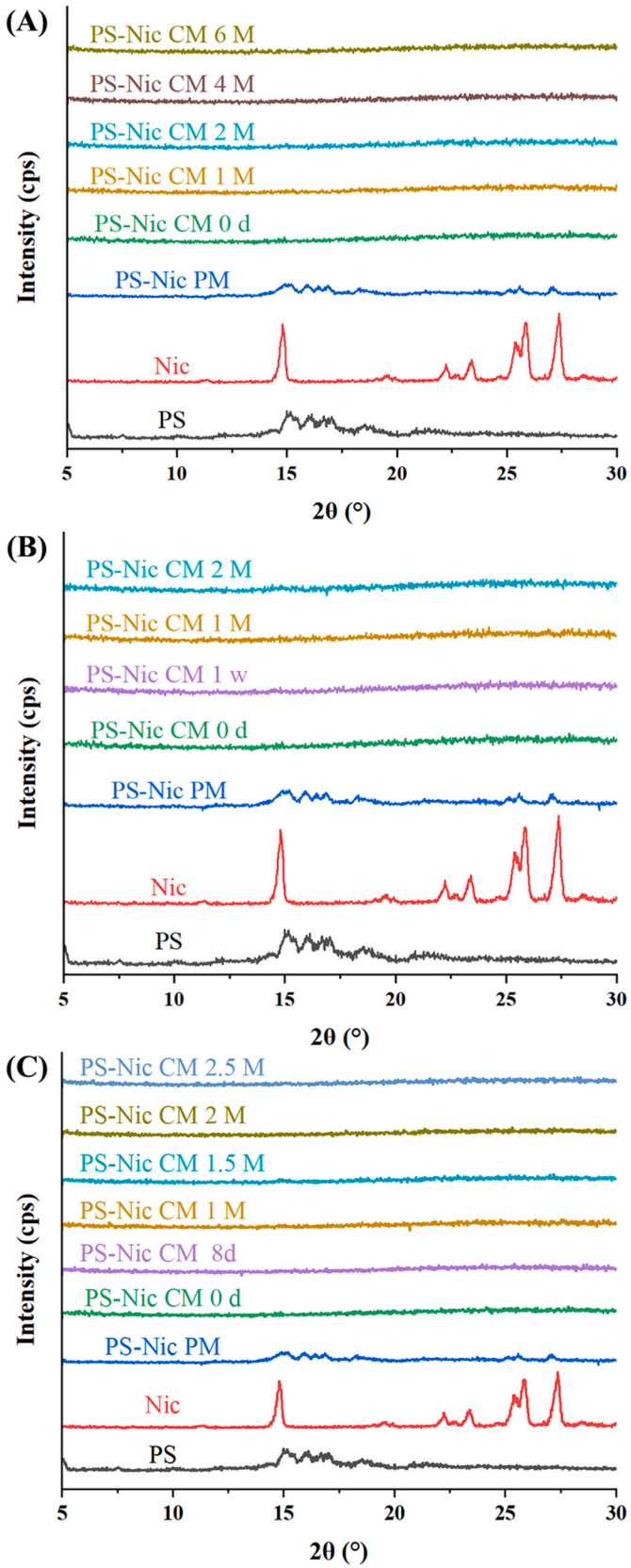

Fig. 7. XRD patterns of 20:1 (w/w) freeze-dried PS-Nic CM at (A) 4 °C (B) 0% RH (i.e., dry), and room temperature, and (C) accelerated storage environment at 40 °C 75% RH to determine its storage stability.

stabilizing it to a certain extent.

4. Conclusions

In this study, we investigated the effect of adding different food-grade coformers, various mixing methods, and different mass ratios of PS-coformers on the solubility of a phytosterol (PS) mixture comprising β-sitosterol, stigmasterol, and campesterol in distilled water. Nicotinamide (Nic) achieved the highest solubility of PS. Specifically, the 20:1 (w/w) PS-Nic co-amorphous mixture prepared via freeze drying (PS-Nic CM) achieved a solubility of 1536.4 μg/mL, which was significantly higher than that of the PS mixture (~0 μg/mL). X-ray diffraction and differential scanning calorimetry revealed that the components in the mixture transformed from the crystalline to the amorphous state after lyophilization. The melting point of CM was not observable, indicating good miscibility of PS and Nic. Compared with PS, PS-Nic CM showed significant changes in morphology with reduced particle size and increased surface area. Fourier-transform infrared, Raman, and ^{1}H NMR spectroscopies revealed intermolecular interactions between PS and Nic. Molecular dynamics simulations confirmed five pairs of intermolecular interactions between the PS (β-sitosterol, stigmasterol, and campesterol) and Nic. Furthermore, the PS-Nic CM demonstrated *in vitro* release of up to 60% within 2 h and stability in the amorphous state after storage at 4 °C for 6 months and after accelerated storage conditions equivalent to room temperature (25 °C) for 10 months. Our findings show that PS-Nic CM has potential applications in food products and can guide the processing of PS in the food industry. Additionally, co-amorphous products could be applied in more diverse food systems to meet nutritional fortification needs. And the low cost of ingredients and simplicity of the process makes it suitable for mass commercial production. Furthermore, the effect of CM products on the physicochemical and organoleptic properties of foods remains unknown and their in vivo bioavailability also needs to be experimentally verified.

CRediT authorship contribution statement

Yuxin Li: Data curation, Writing – original draft. **Yingting Luo:** Formal analysis, Visualization, Software. **Xuening Song:** Methodology, Validation. **Yuzhuo Wang:** Methodology, Validation. **Simiao Liu:** Methodology, Validation. **Fazheng Ren:** Resources, Investigation. **Lingyan Kong:** Writing – review & editing. **Hao Zhang:** Supervision, Writing – review & editing, Project administration, Funding acquisition.

Funding sources

This work was supported by National Key R&D Program of China (No. 2022YFF1100402.)

Declaration of competing interest

The authors declare that they have no known competing financial interests or personal relationships that could have appeared to influence the work reported in this paper.

Data availability

Data will be made available on request.

References

Acevedo-Estupiñan, M.V., Gutierrez-Lopez, G.F., Cano-Sarmiento, C., Parra-Escudero, C. O., Rodriguez-Estrada, M.T., Garcia-Varela, R., García, H.S., 2019. Stability and characterization of o/w free phytosterols nanoemulsions formulated with an enzymatically modified emulsifier. Lwt 107, 151–157. https://doi.org/10.1016/j.lwt.2019.03.004.

Ahuja, N., Katare, O.P., Singh, B., 2007. Studies on dissolution enhancement and mathematical modeling of drug release of a poorly water-soluble drug using water-

soluble carriers. Eur. J. Pharm. Biopharm. 65 (1), 26–38. https://doi.org/10.1016/j.ejpb.2006.07.007.
Alvarez-Henao, M.V., León, D.E., Londoño-Londoño, J., Jimenez-Cartagena, C., 2023. Spray drying of phytosterols: an alternative to improve the solubility of bioactive ingredients, with application in food matrices. J. Food Process. Eng. 46 (11), e14307. https://doi.org/10.1111/jfpe.14307.
Asare-Addo, K., Alshafiee, M., Walton, K., Ward, A., Totea, A., Taheri, S., Mawla, N., Adebisi, A.O., Elawad, S., Diza, C., Timmins, P., Conway, B.R., 2019. Effect of preparation method on the surface properties and UV imaging of indomethacin solid dispersions. Eur. J. Pharm. Biopharm. 137, 148–163. https://doi.org/10.1016/j.ejpb.2019.03.002.
Bhagwat, A., Pathan, I.B., Chishti, N.A.H., 2021. Design and optimization of pellets formulation containing curcumin ascorbic acid co-amorphous mixture for ulcerative colitis management. Part. Sci. Technol. 39 (7), 859–867. https://doi.org/10.1080/02726351.2020.1848946.
Biniek, K., Tfayli, A., Vyumvuhore, R., Quatela, A., Galliano, M., Delalleau, A., Baillet-Guffroy, A., Dauskardt, R.H., Duplan, H., 2018. Measurement of the biomechanical function and structure of ex vivo drying skin using Raman spectral analysis and its modulation with emollient mixtures. Exp. Dermatol. 27 (8), 901–908. https://doi.org/10.1111/exd.13721.
Borde, S., Hegde, P., Prathipati, P., North, J., Kumari, D., Chauhan, H., 2021. Formulation and characterization of ternary amorphous solid dispersions of a highly potent anti-tubercular agent and curcumin. J. Drug Deliv. Sci. Technol. 64, 102564. https://doi.org/10.1016/j.jddst.2021.102564.
Careri, M., Elviri, L., Mangia, A., 2001. Liquid chromatography–UV determination and liquid chromatography–atmospheric pressure chemical ionization mass spectrometric characterization of sitosterol and stigmasterol in soybean oil. J. Chromatogr., A 935 (1), 249–257. https://doi.org/10.1016/S0021-9673(01)01079-2.
De Stefani, E., Boffetta, P., Ronco, A.L., Brennan, P., Deneo-Pellegrini, H., Carzoglio, J.C., Mendilaharsu, M., 2000. Plant sterols and risk of stomach cancer: a case-control study in Uruguay. Nutr. Cancer 37 (2), 140–144. https://doi.org/10.1207/S15327914NC372_4.
Ding, F., Cao, W., Wang, R., Wang, N., Li, A., Wei, Y., Qian, S., Zhang, J., Gao, Y., Pang, Z., 2023. Mechanistic study on transformation of coamorphous baicalein-nicotinamide to its cocrystal form. J. Pharmaceut. Sci. 112 (2), 513–524. https://doi.org/10.1016/j.xphs.2022.08.031.
Feng, S., Yan, J., Wang, D., Jiang, L., Sun, P., Xiang, N., Shao, P., 2021. Preparation and characterization of soybean protein isolate/pectin-based phytosterol nanodispersions and their stability in simulated digestion. Food Res. Int. 143, 110237. https://doi.org/10.1016/j.foodres.2021.110237.
Gan, C., Liu, Q., Zhang, Y., Shi, T., He, W., Jia, C., 2022. A novel phytosterols delivery system based on sodium caseinate-pectin soluble complexes: improving stability and bioaccessibility. Food Hydrocolloids 124, 107295. https://doi.org/10.1016/j.foodhyd.2021.107295.
Garbiec, E., Rosiak, N., Tykarska, E., Zalewski, P., Cielecka-Piontek, J., 2023. Sinapic acid co-amorphous systems with amino acids for improved solubility and antioxidant activity. Int. J. Mol. Sci. 24 (6), 5533. https://doi.org/10.3390/ijms24065533.
Hancock, B.C., Zografi, G., 1997. Characteristics and significance of the amorphous state in pharmaceutical systems. J. Pharmaceut. Sci. 86 (1), 1–12. https://doi.org/10.1021/js9601896.
He, W., Ma, Y., Pan, X., Li, J., Wang, M., Yang, Y., Jia, C., Zhang, X., Feng, B., 2012. Efficient solvent-free synthesis of phytostanyl esters in the presence of acid-surfactant-combined catalyst. J. Agric. Food Chem. 60 (38), 9763–9769. https://doi.org/10.1021/jf302958g.
He, Y., Liu, H., Bian, W., Liu, Y., Liu, X., Ma, S., Zheng, X., Du, Z., Zhang, K., Ouyang, D., 2019. Molecular interactions for the curcumin-polymer complex with enhanced anti-inflammatory effects. Pharmaceutics 11 (9), 442. https://doi.org/10.3390/pharmaceutics11090442.
Heinz, A., Strachan, C.J., Gordon, K.C., Rades, T., 2009. Analysis of solid-state transformations of pharmaceutical compounds using vibrational spectroscopy. J. Pharm. Pharmacol. 61 (8), 971–988. https://doi.org/10.1211/jpp.61.08.0001.
Jangid, A.K., Jain, P., Medicherla, K., Pooja, D., Kulhari, H., 2020. Solid-state properties, solubility, stability and dissolution behaviour of co-amorphous solid dispersions of baicalin. CrystEngComm 22 (37), 6128–6136. https://doi.org/10.1039/D0CE00750A.
Kamiya, S., Kurita, T., Miyagishima, A., Itai, S., Arakawa, M., 2010. Physical properties of griseofulvin-lipid nanoparticles in suspension and their novel interaction mechanism with saccharide during freeze-drying. Eur. J. Pharm. Biopharm. 74 (3), 461–466. https://doi.org/10.1016/j.ejpb.2009.12.004.
Kasten, G., Löbmann, K., Grohganz, H., Rades, T., 2019. Co-former selection for co-amorphous drug-amino acid formulations. Int. J. Pharm. 557, 366–373. https://doi.org/10.1016/j.ijpharm.2018.12.036.
Li, B., Hu, Y., Wu, T., Feng, Y., Jiang, C., Du, H., Lu, S., 2022. Apigenin-oxymatrine binary co-amorphous mixture: enhanced solubility, bioavailability, and anti-inflammatory effect. Food Chem. 373, 131485. https://doi.org/10.1016/j.foodchem.2021.131485.
Lim, L.M., Park, J., Hadinoto, K., 2022. Benchmarking the solubility enhancement and storage stability of amorphous drug–polyelectrolyte nanoplex against co-amorphous formulation of the same drug. Pharmaceutics 14 (5), 979. https://doi.org/10.3390/pharmaceutics14050979.
Lin, H., Zhang, G., Huang, Y., Lin, S., 2014. An investigation of indomethacin–nicotinamide cocrystal formation induced by thermal stress in the solid or liquid state. J. Pharmaceut. Sci. 103 (8), 2386–2395. https://doi.org/10.1002/jps.24056.
Liu, L., Xu, Y., Chen, F., Zhang, S., Li, L., Ban, Z., 2023. Soy proteins as vehicles for enhanced bioaccessibility and cholesterol-lowering activity of phytosterols. J. Sci. Food Agric. 103 (1), 205–212. https://doi.org/10.1002/jsfa.12132.
Liu, X., Lu, M., Guo, Z., Huang, L., Feng, X., Wu, C., 2012. Improving the chemical stability of amorphous solid dispersion with cocrystal technique by hot melt extrusion. Pharm. Res. (N. Y.) 29 (3), 806–817. https://doi.org/10.1007/s11095-011-0605-4.
Matsuoka, R., 2022. Property of phytosterols and development of its containing mayonnaise-type dressing. Foods 11 (8), 1141. https://doi.org/10.3390/foods11081141.
Matsuoka, R., Masuda, Y., Takeuchi, A., Marushima, R., Onuki, M., 2004. Minimal effective dose of plant sterol on serum cholesterol concentration in Japanese subjects and safety evaluation of plant sterol supplemented in mayonnaise. J. Oleo Sci. 53 (1), 17–27. https://doi.org/10.5650/jos.53.17.
Mccann, S.E., Freudenheim, J.L., Graham, S., Marshall, J.R., 2003. Risk of human ovarian cancer is related to dietary intake of selected nutrients, phytochemicals and food groups. J. Nutr. 133 (6), 1937–1942. https://doi.org/10.1093/jn/133.6.1937.
Meng, F., Trivino, A., Prasad, D., Chauhan, H., 2015. Investigation and correlation of drug polymer miscibility and molecular interactions by various approaches for the preparation of amorphous solid dispersions. Eur. J. Pharmaceut. Sci. 71, 12–24. https://doi.org/10.1016/j.ejps.2015.02.003.
Meng, X., Pan, Q., Liu, Y., 2012. Preparation and properties of phytosterols with hydroxypropyl β-cyclodextrin inclusion complexes. Eur. Food Res. Technol. 235 (6), 1039–1047. https://doi.org/10.1007/s00217-012-1833-5.
Moreau, R.A., Nyström, L., Whitaker, B.D., Winkler-Moser, J.K., Baer, D.J., Gebauer, S. K., Hicks, K.B., 2018. Phytosterols and their derivatives: structural diversity, distribution, metabolism, analysis, and health-promoting uses. Prog. Lipid Res. 70, 35–61. https://doi.org/10.1016/j.plipres.2018.04.001.
Muthu, M.J., Kavitha, K., Chitra, K.S., Nandhineeswari, S., 2019. Soluble curcumin prepared by solid dispersion using four different carriers: phase solubility, molecular modelling and physicochemical characterization. Trop. J. Pharmaceut. Res. 18 (8), 1581–1588. https://doi.org/10.4314/tjpr.v18i8.2.
Oyama, S., Ogawa, N., Kawai, K., Iwai, K., Yasunaga, T., Yamamoto, H., 2024. Improved dissolution properties of co-amorphous probucol with atorvastatin calcium trihydrate prepared by spray-drying. Chem. Pharm. Bull. 72 (2), 190–199. https://doi.org/10.1248/cpb.c23-00673.
Pal, T., Narayanan, V.A., Stokes, D.L., Vo-Dinh, T., 1998. Surface-enhanced Raman detection of nicotinamide in vitamin tablets. Anal. Chim. Acta 368 (1), 21–28. https://doi.org/10.1016/S0003-2670(98)00192-5.
Pham, D.T.T., Tran, P.H.L., Tran, T.T.D., 2019. Development of solid dispersion lipid nanoparticles for improving skin delivery. Saudi Pharmaceut. J. 27 (7), 1019–1024. https://doi.org/10.1016/j.jsps.2019.08.004.
Ribeiro, H.S., Gupta, R., Smith, K.W., van Malssen, K.F., Popp, A.K., Velikov, K.P., 2016. Super-cooled and amorphous lipid-based colloidal dispersions for the delivery of phytosterols. Soft Matter 12 (27), 5835–5846. https://doi.org/10.1039/C6SM00601A.
Rozner, S., Popov, I., Uvarov, V., Aserin, A., Garti, N., 2009. Templated cocrystallization of cholesterol and phytosterols from microemulsions. J. Cryst. Growth 311 (16), 4022–4033. https://doi.org/10.1016/j.jcrysgro.2009.06.027.
Song, X., Luo, Y., Zhao, W., Liu, S., Wang, Y., Zhang, H., 2024. Preparation and characterization of lutein co-amorphous formulation with enhanced solubility and dissolution. Foods 13 (13), 2029. https://doi.org/10.3390/foods13132029.
Tawfeek, H.M., Chavan, T., Kunda, N.K., 2020. Effect of spray drying on amorphization of indomethacin nicotinamide cocrystals; Optimization, characterization, and stability study. AAPS PharmSciTech 21 (5), 181. https://doi.org/10.1208/s12249-020-01732-x.
Telange, D.R., Patil, A.T., Pethe, A.M., Fegade, H., Anand, S., Dave, V.S., 2017. Formulation and characterization of an apigenin-phospholipid phytosome (APLC) for improved solubility, in vivo bioavailability, and antioxidant potential. Eur. J. Pharmaceut. Sci. 108, 36–49. https://doi.org/10.1016/j.ejps.2016.12.009.
Turek, M., Różycka-Sokołowska, E., Koprowski, M., Marciniak, B., Bałczewski, P., 2021. Role of hydrogen bonds in formation of co-amorphous valsartan/nicotinamide compositions of high solubility and durability with anti-hypertension and anti-COVID-19 potential. Mol. Pharm. 18 (5), 1970–1984. https://doi.org/10.1021/acs.molpharmaceut.0c01096.
Wegiel, L.A., Zhao, Y., Mauer, L.J., Edgar, K.J., Taylor, L.S., 2014. Curcumin amorphous solid dispersions: the influence of intra and intermolecular bonding on physical stability. Pharmaceut. Dev. Technol. 19 (8), 976–986. https://doi.org/10.3109/10837450.2013.846374.
Yamamura, S., Gotoh, H., Sakamoto, Y., Momose, Y., 2000. Physicochemical properties of amorphous precipitates of cimetidine–indomethacin binary system. Eur. J. Pharm. Biopharm. 49 (3), 259–265. https://doi.org/10.1016/S0939-6411(00)00060-6.
Yang, R., Li, Y., Li, J., Liu, C., Du, P., Zhang, T., 2018. Application of scCO2 technology for preparing CoQ10 solid dispersion and SFC-MS/MS for analyzing in vivo bioavailability. Drug Dev. Ind. Pharm. 44 (2), 289–295. https://doi.org/10.1080/03639045.2017.1391833.
Yang, R., Xue, L., Zhang, L., Wang, X., Qi, X., Jiang, J., Yu, L., Wang, X., Zhang, W., Zhang, Q., Li, P., 2019. Phytosterol contents of edible oils and their contributions to estimated phytosterol intake in the Chinese diet. Foods 8 (8), 334. https://doi.org/10.3390/foods8080334.
Zhang, Q., Polyakov, N.E., Chistyachenko, Y.S., Khvostov, M.V., Frolova, T.S., Tolstikova, T.G., Dushkin, A.V., Su, W., 2018. Preparation of curcumin self-micelle solid dispersion with enhanced bioavailability and cytotoxic activity by mechanochemistry. Drug Deliv. 25 (1), 198–209. https://doi.org/10.1080/10717544.2017.1422298.